Journal of ELECTRONIC MATERIALS, Vol. 48, No. 10, 2019
https://doi.org/10.1007/s11664-019-07487-x

The Magnetic, Electrical and Optical Properties of Rare Earth Er^{3+} Doped Lead Borate Glass

MOHAMMAD AHMAD-FOUAD BASHA,[1,4]
REHAM MORSI MOHAMED MORSI,[2] MORSI MOHAMED MORSI,[3]
and AHMAD FOUAD BASHA[1]

1.—Physics Department, Faculty of Science, Cairo University, P.O. Box 12613, Giza, Egypt. 2.—Physical Chemistry Department, National Research Centre, 33 El Bohoth Street (Former El Tahrir Street), Dokki, P.O. Box 12622, Giza, Egypt. 3.—Glass Research Department, National Research Centre, 33 El Bohoth Street (Former El Tahrir Street), Dokki, P.O. Box 12622, Giza, Egypt. 4.—e-mail: mafbasha@sci.cu.edu.eg

Owing to the unique electronic structure of rare earth elements, we address in this paper the magnetic, electrical and optical properties of a prepared lead borate glass of composition (mol.%) $70PbO{\cdot}30B_2O_3$. The glass is doped with different $ErCl_3$ contents. A vibrating-sample magnetometer was used to characterize the magnetic properties. Increasing the additive concentration led to an increase in the saturation magnetization without significant effects on the coercivity. Optical reflectance spectra of the doped glasses revealed the development of absorption bands as a result of Er^{3+} intra-configurational (*f–f*) transitions. The calculated allowed direct energy gap was found to increase monotonically with increasing dopant concentration. The results of the ac conductivity showed a decrease in the activation energy values with increasing frequency and an increase in the ac conductivity values with increasing temperature, which mimics the semiconducting behavior. The incorporation of the rare earth ion (Er^{3+}) facilitated the electronic conduction due to the increase of the non-bridging oxygen units. Increasing the dopant concentration led also to the participation of the ionic conductions. However, further increase of $ErCl_3$ (above 1 mol.%) caused a decrease in the conductivity. Samples with dopant content up to 1 mol.% $ErCl_3$ are accompanied by a high dielectric constant value of about 40. It can be concluded that samples doped with 1 mol.% $ErCl_3$ or less can be used as energy storage material in electronic devices, whereas glass samples with higher dopant content can be used for magnetic applications.

Key words: Lead borate glasses, rare earth elements, magnetic properties, optical properties, electrical properties, A.C. conductivity

INTRODUCTION

Nowadays, use of glass materials has evolved from the simple conventional passive functions to more sophisticated active functions in many optical, electronic, structural, chemical and biochemical interdisciplinary applications.[1] The importance of developing new types of glass with more active functions has recently received great attention and extensive work has been carried out on the design of new glass compositions with particular emphasis on rare-earth-doped transparent glass systems that are characterized by various unique properties.[2–4]

Heavy metal borate glass systems, which are based on heavy metal ions during their preparation, are characterized by high refractive indices and higher transmission in the infrared region.[5,6] They have received great attention for their expected use

(Received January 19, 2019; accepted July 25, 2019; published online August 2, 2019)

in the development of all-optical technology towards faster data communication.[7,8] It is reported that these borate glasses have high phonon energies and they are the most suitable for hosting rare earth metals such as erbium.[9,10]

Trivalent erbium-doped glasses have exceptional optical fluorescent properties that are particularly useful in certain applications, such as near-infrared solid-state laser media, optical amplifiers and NIR-to-visible up-converted systems.[11–14] Extensive work has been performed on the emission properties of Er^{3+}-doped glasses for photonic and optoelectronic applications.[5,15–19] Er^{3+}-borate glass containing bismuth oxide has been explored for the effect of glass composition on the thermal, structural, optical and NIR emission spectroscopic properties.[20,21] Erbium oxide has been reported to act as a glass-modifier and influencer on the $BO_3 \leftrightarrow BO_4$ conversion.[22]

Less attention has been given to the magnetic and electrical properties of Er^{3+} doped glass systems. However, it is reported that introducing Er^{3+} ions into some amorphous and semi-crystalline polymer systems may result in improving the dielectric and relaxation properties of such systems.[23–25] Accordingly, the aim of the present work is to focus on the magnetic, electrical and optical properties of a binary lead-borate glass containing different concentrations of Er^{3+} ions.

EXPERIMENTAL

Lead borate glasses, based on the composition (mol.%) $70PbO{\cdot}30B_2O_3$ and doped with $ErCl_3$, were prepared via melt quenching. Red lead oxide and anhydrous boric acid (BDH Chemicals Company, Japan.), $ErCl_3{\cdot}6H_2O$ (99.9%, purity, Strem Chemicals Inc., Newburyport, MA, USA) were used in the preparation of the glass samples. Batches with different concentrations of 0.1, 1, 10, 15 and 20 mol.% $ErCl_3$ were melted in porcelain crucibles for half an hour at 950°C in an electrically heated furnace under air conditions. The samples obtained were treated as described elsewhere[26] and are referred to as BP-0.1, BP-1, BP-10, BP-15 and BP-20, respectively. Most samples were visually dark in color. The dopant-free glass sample is given the code number BP-0.0.

The M-H hysteresis loops were measured on a vibrating-sample magnetometer (VSM) of the type VSM-9600-1 (LDI Electronics, Troy, MI, USA) at room temperature and by using flux densities of the applied magnetic fields up to 20 kG.

The diffused reflectance spectra were measured in the range of 190–1100 nm on unpolished light-scattered glass samples using a double beam UV/Vis spectrophotometer, PerkinElmer LAMBDA 35 equipped with a 50 mm integrating sphere. The data obtained from the diffused reflectance curves were used to investigate the optical energy gap based on Kubelka–Munk parameters.

Electrical measurements were performed on the prepared samples after painting the opposite surfaces with silver paste. A programmable automatic LCR Hi-Tester (HIOKI, 3532-50), Japan, was used over a frequency range from 0.042 kHz to 1 MHz and at temperature range of 298 K to 573 K. The temperature was determined using a copper/constantan thermocouple in close proximity to the sample. The values of dielectric constant (ε') and ac conductivity (σ_{ac}) were determined using the following expressions[27–29]: $\varepsilon' = Cd/\varepsilon_0 A$, $\varepsilon'' = \varepsilon' \tan\delta$ and $\sigma_{ac} = \omega\varepsilon_0\varepsilon''$, where C is the measured capacitance of the sample in Farads, d is the thickness of the sample in meters, ε_0 is the permittivity of free space, which equals to 8.85×10^{-12} Fm^{-1}, A is the sample's surface area in m^2, ω is the angular frequency and $\tan\delta$ is the loss tangent, which is obtained directly from the instrument.

RESULTS AND DISCUSSION

Magnetic Properties

To study the effect of the additive concentration on the magnetic properties of the glass samples, hysteresis loops for the glass samples BP-1, BP-10, BP-15 and BP-20 were measured at room temperature and plotted in Fig. 1. It is clear from the figure that the alignment of the magnetic dipoles, due to the external applied magnetic field, exhibits irreversible behavior and leaves remnant magnetization when the applied field is zero, for all the glass samples. This behavior is similar to that of ferromagnetic materials.[30] Moreover, the hysteresis curve for the glass sample BP-1 exhibits an ideal S shaped structure, which is a characteristic behavior of ferrimagnetism.[31] The magnetic parameters, the saturation magnetization (M_s), the remnant magnetization (M_r), the squareness (SQR = M_r/M_s) and the coercivity (H_c), can be determined from the hysteresis loops in Fig. 1. Also, the dissipated energy per mass (A) can be obtained, which is equal to the area enclosed by the hysteresis loops.

For the BP-10, BP-15 and BP-20 glass samples, the saturation magnetization was found to be beyond the range of the applied field, so to calculate M_s properly, a relation between the magnetization and the inverse of the field was plotted and the tail of the magnetization curve was extrapolated to intersect with the magnetization axis where the inverse of the field is equal to zero. The obtained magnetic parameters are represented in Table I.

It is noticed from Fig. 1 that, as the concentration of Er^{3+} increases, the saturation magnetization increases without a significant change in the coercivity. Moreover, the correlation between the saturation magnetization and the concentration of the additives follows a linear trend, as seen in the inset of Fig. 1, which indicates that the process of magnetization has not resulted in any loss in magnetic

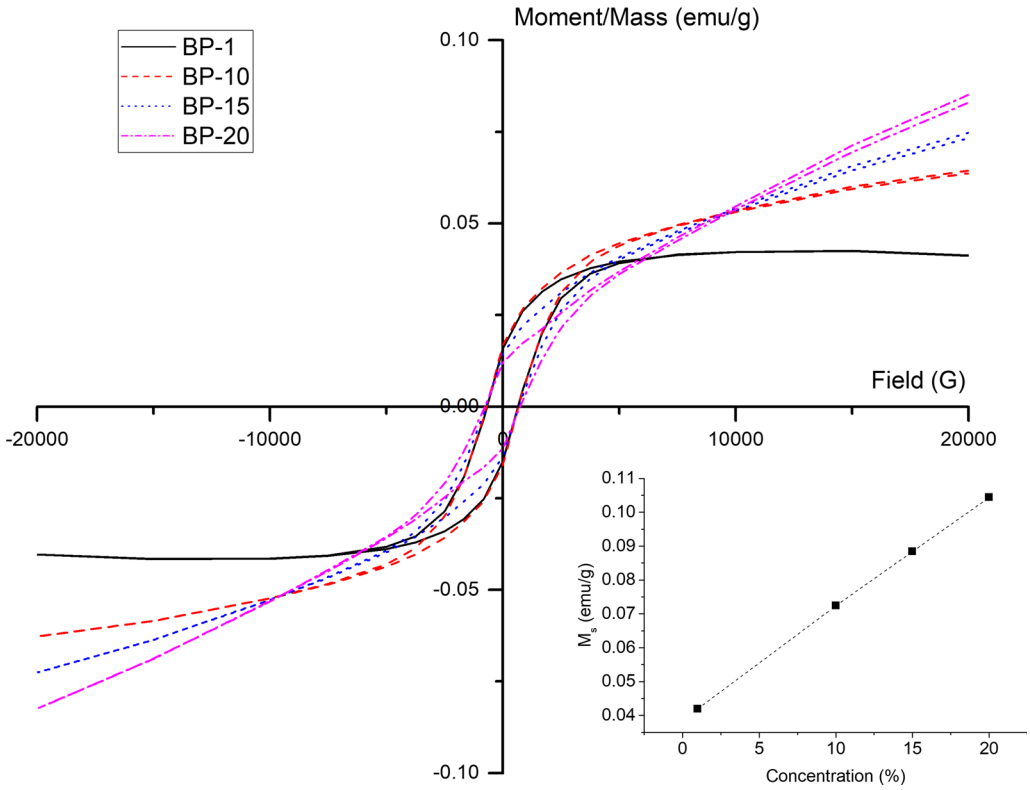

Fig. 1. Hysteresis loops from VSM measurements for BP-1, BP-10, BP-15 and BP-20 glass samples. The inset indicates the change of the saturation magnetization M_s with the concentration of the $ErCl_3$.

Table I. The values of the area of the hysteresis loop (A), the coercivity (H_c), the remnant magnetization (M_r), the saturation magnetization (M_s) and the squareness (SQR = M_r/M_s)

Sample	A (erg/g)	H_c (G)	M_r (emu/g)	M_s (emu/g)	SQR
BP-1	97.29	665.42	0.01582	0.04194	0.3772
BP-10	110.30	729.59	0.01681	0.07241	0.2322
BP-15	101.62	729.59	0.01449	0.08839	0.1639
BP-20	93.03	737.99	0.01213	0.10438	0.1162

properties of the magnetic particles and the observed variation in the M_s value of different samples is only a result of increasing the content of magnetic material in the glass samples.[32] This interesting results indicate that by increasing the dopant concentration, these glass samples could be more desirable for applications that require relatively higher magnetic permeability.[33,34] The reduced M_s in these samples may restrict their applications; however, their high coercivity values may make it a promising candidate for some applications such as in electric compasses and position sensors, magnetic detectors, magnetic sources in medical applications, speakers and audio systems that work without power supply. The increase in M_s with increasing Er^{3+} concentration may be interpreted by the increase of the unpaired electrons, which provide a large net magnetism when the sample is placed in a magnetic field.[35]

Optical Properties

Figure 2 shows the diffused reflectance spectra of the prepared $ErCl_3$ doped lead borate glasses in the range 200–500 nm, as no important features were recorded at longer wavelengths.

The absorption peaks appear in the reflection measurements as saddles and they were labelled by the values of their position on the wavelength axis. A plot of $F(R)$, which is proportional to the absorption coefficient, for sample BP-1 is included as inset in Fig. 2 to confirm the positions of the peaks observed in the reflectance spectra. The spectrum of un-doped glass (Fig. 2) reveals the presence of absorption bands at 224, 289 and 340 nm. The bands at 224 nm can be considered one of the bands that constitute the UV cut-off. It shifts to longer wavelengths with increasing dopant content up to 1% to reach a value of 230 nm, then shifts to a shorter wavelength to reach 224 nm for a doping

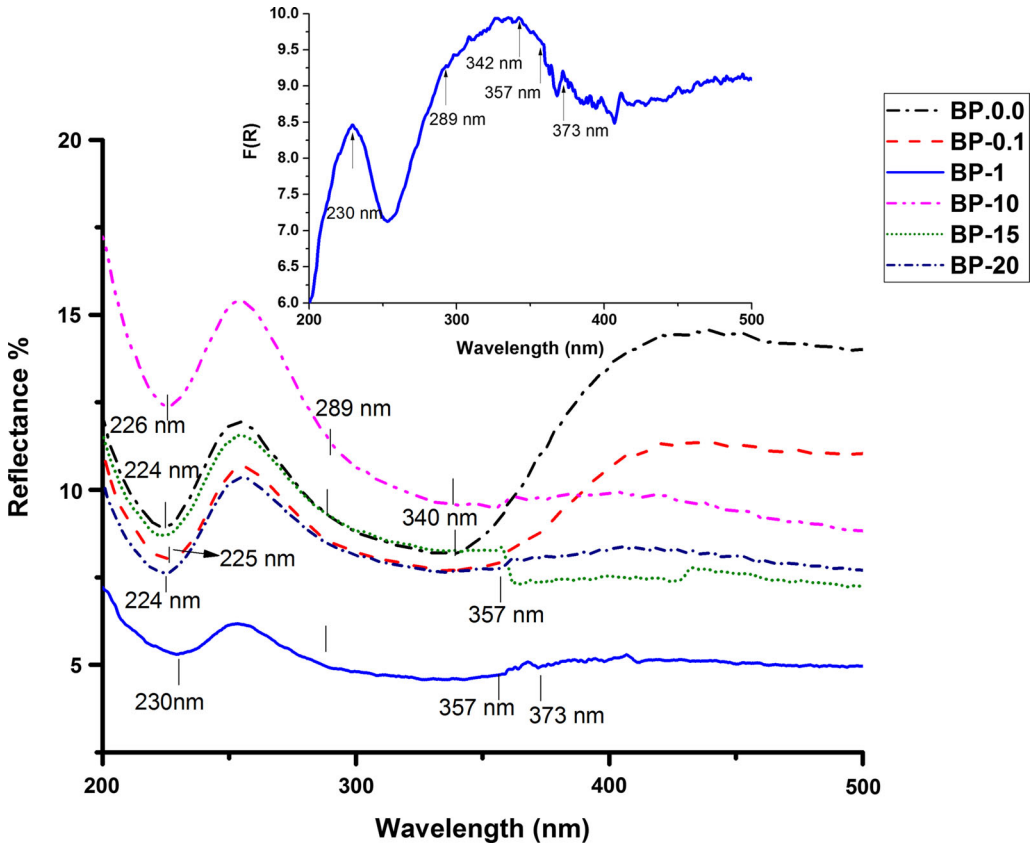

Fig. 2. Diffused reflectance spectra of the studied glasses. The inset shows the $F(R)$ plot for sample BP-1, which confirms the positions of the peaks observed in the reflectance spectra.

content of 20%. The band at 289 nm can be assigned to charge transfer associated with Pb^{2+} and their neighboring ligands.[36] The absorption band at 340 nm is near that recorded for the UV cut off appeared at 347 nm in a binary lead borate glass and related to electron transitions of non-bridging oxygen anions in the glass.[37]

The observed spectra of the doped glasses indicate the development of weak absorption bands at 357 and 373 nm which are due to Er^{3+} arising from the intra-configurational (f–f) transition.[38] The absorption bands at 357 nm and 373 nm can be correlated with those due to $2G_{9/2}$ and $4G_{11/2}$ at 363 nm and 377 nm, respectively.[39]

It is reported that in the range 400–550 nm, several absorption bands due to Er-ions were observed in the multicomponent PbO-B_2O_3-Al_2O_3-WO_3 glass system.[22] The disappearance of those bands in the recorded spectra of the presented binary glass system (Fig. 2) can be attributed to the decrease of the crystal field strength at the rare-earth sites. The investigated glasses contain high PbO content, which causes an increase of the Ln^{3+}-O covalency.[40] The increased covalency is expected to lead to more symmetrical field strength around the 4f electrons, consequently a decrease of the crystal field strength.

The Tauc Plots

For an electron to be excited from the highest occupied molecular orbital to the lowest unoccupied molecular orbital, it needs to absorb a photon with an amount of energy equal to the energy difference between the two energy levels. The wavelength of the absorbed photon is calculated by $E = h\upsilon$, where E is the energy of the absorbed photon, h is Planck's constant and υ is the frequency of the electromagnetic wave associated to the photon.

We can calculate the band gap energy by modeling the reflectance spectrum using the Kubelka–Munk method, which allows the calculation of reflectance. In this method, we used the Kubelka–Munk function $F(R)$ to plot the Tauc plots, by calculating this function from the relation[41–45]:

$$F(R) = \frac{(1-R)^2}{2R}, \tag{1}$$

where R is the reflectance. The Tauc plots are expressed by the following relation[46,47]:

$$(\alpha E)^{1/r} = A(E - E_g), \tag{2}$$

where α is the absorption coefficient, E_g is the band gap energy and A is the proportionality constant. The exponent r used in the Tauc plots can assume

different integer values for the different types of transitions. For the allowed direct transitions, $r = 1/2$ and in this case $E_g = E_d$, whereas for the allowed indirect transition, $r = 2$ where $E_g = E_{in}$. Since the quantity $F(R)$ is proportional to the absorption coefficient α, we can consider Tauc relation as follows[45]:

$$[F(R)E]^{1/r} = A(E - E_g) \quad (3)$$

The modified Tauc relations, using $r = 1/2$ for allowed direct transitions and $r = 2$ for allowed indirect transitions, are plotted in Figs. 3 and 4, respectively. The linear part in the Tauc plots was fitted by a straight line function to find the intersection with the E axis, which gives the band gap energy for the corresponding transition type.

The values of the direct band gaps E_d and the indirect ones E_{in} for the glass samples, as determined from the fitting results, are listed in Table II. It can be noticed that after the first addition of $ErCl_3$ both the allowed direct and indirect energy gaps decrease with increasing the additive concentration up to 1% $ErCl_3$ then increase monotonically with increasing the additive concentration as depicted from Fig. 5. The observed decrease is accompanied with a shift of the optical absorption band in the UV region to longer wavelengths then to shorter ones with increasing the dopant content (Fig. 2). The data of E_{opt} seems to arise due to the allowed transitions. In un-doped binary $30B_2O_3$-$70PbO_2$ glass the optical band gap was reported to arise as a result of direct forbidden transition.[48]

AC Electrical Properties

Figure 6 shows the dependence of the ac conductivity on temperature for all the studied glass samples at selected frequencies (1 kHz, 100 kHz and 1 MHz). The results obtained indicate that ac conductivity values increase with increasing temperature, which reveals that the present samples are semiconducting in nature.[49]

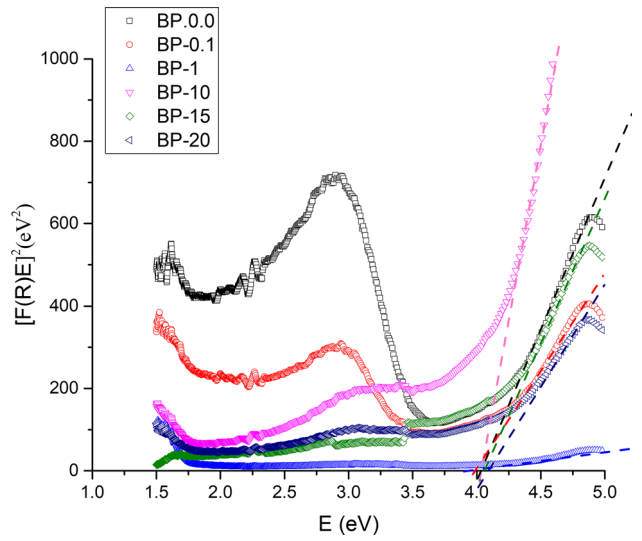

Fig. 3. Tauc plots of $[F(R)E]^2$ versus E for the allowed direct transitions.

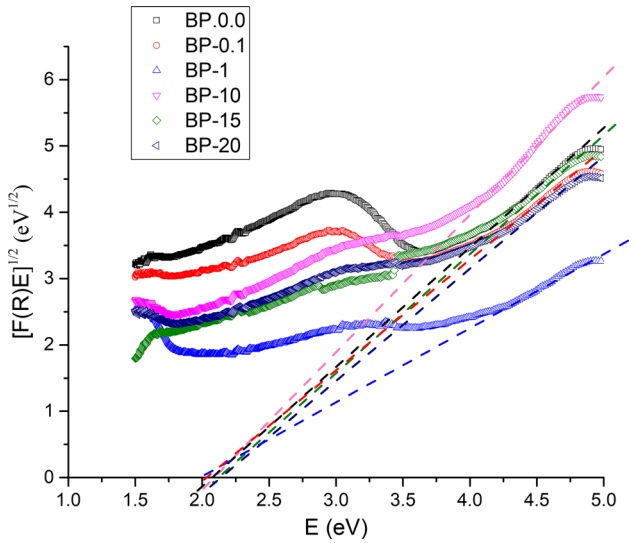

Fig. 4. Tauc plots of $[F(R)E]^{1/2}$ versus E for the allowed indirect transitions.

Table II. The values of the direct band gaps E_d and the indirect band gaps E_{in}

Sample	$ErCl_3 \cdot 6H_2O$[a]	E_d (eV)	E_{in} (eV)
BP-00	0.00	4.03 ± 0.0231	2.08 ± 0.0499
BP-01	0.01	3.99 ± 0.0305	2.04 ± 0.0296
BP-1	1.00	3.94 ± 0.0181	1.98 ± 0.0744
BP-10	10.00	4.04 ± 0.0046	2.09 ± 0.0337
BP-15	15.00	4.06 ± 0.0089	2.12 ± 0.0463
BP-20	20.00	4.09 ± 0.0202	2.14 ± 0.0331

[a]Added weight in mol.%.

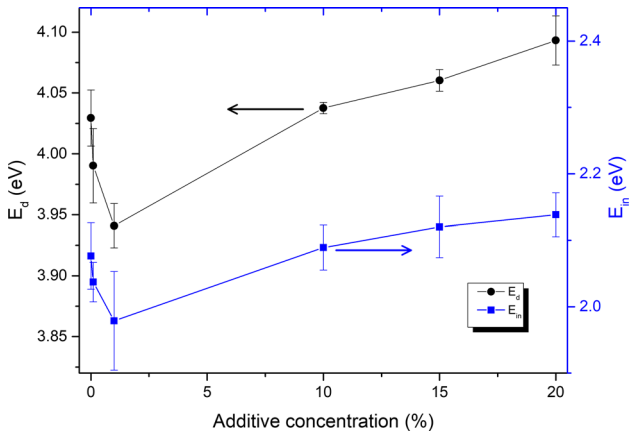

Fig. 5. The direct band gap (E_d) and indirect band gap (E_{in}) as a function of the added $ErCl_3$ concentration.

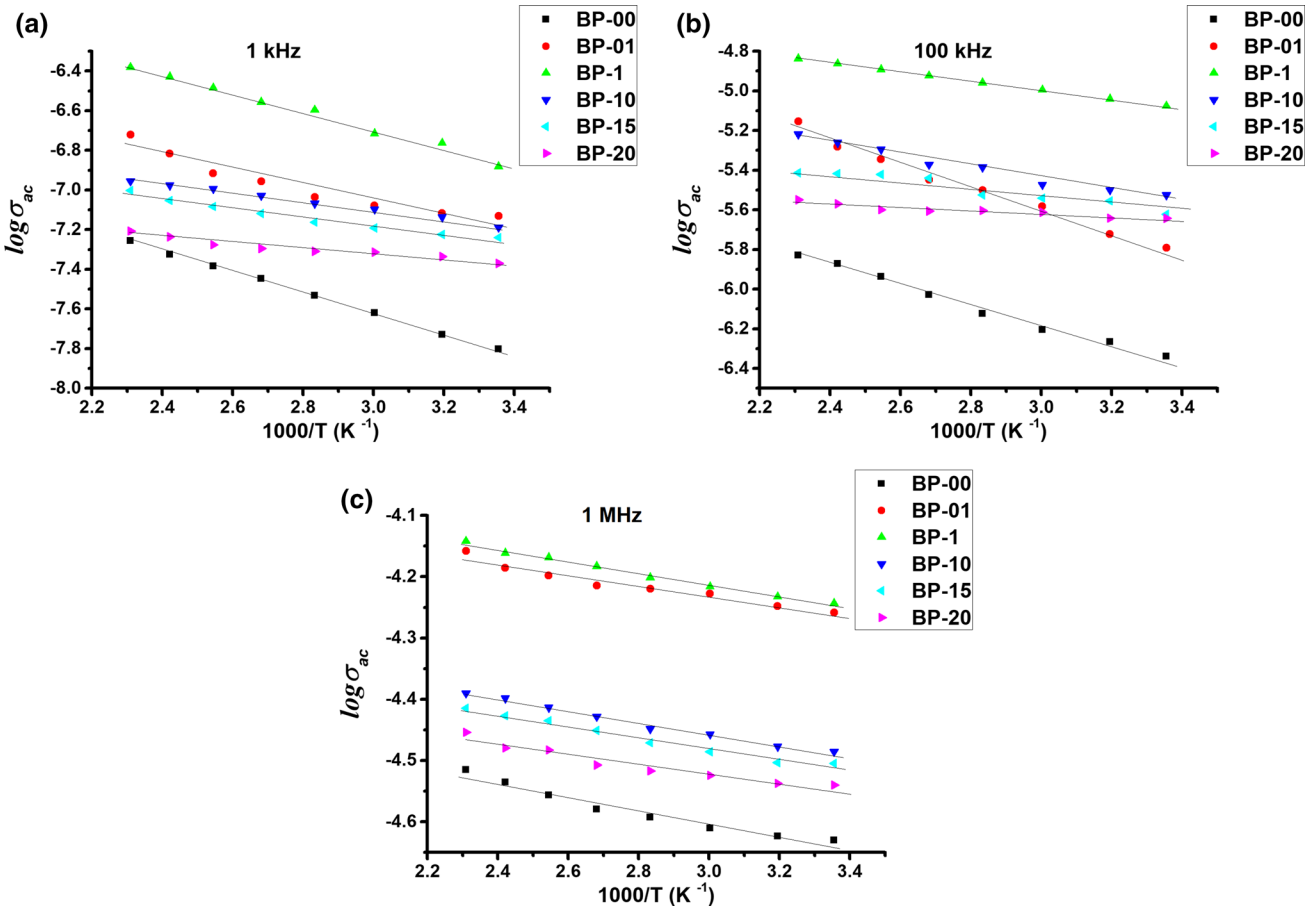

Fig. 6. Temperature dependence of ac conductivity for all glass samples at 1 kHz (a), 100 kHz (b) and 1 MHz (c).

Table III. The values of ac conductivity (σ_{ac}) and the activation energy (E_{ac}) at different frequencies

	1 kHz		100 kHz		1 MHz	
Sample	σ_{ac} ($\Omega^{-1}m^{-1}$)[a]	E_{ac} (eV)	σ_{ac} ($\Omega^{-1}m^{-1}$)[a]	E_{ac} (eV)	σ_{ac} ($\Omega^{-1}m^{-1}$)[a]	E_{ac} (eV)
BP-00	5.77×10^{-8}	0.53 ± 0.0059	4.58×10^{-7}	0.50 ± 0.0205	2.34×10^{-5}	0.11 ± 0.0098
BP-01	4.27×10^{-8}	0.38 ± 0.0478	1.61×10^{-6}	0.58 ± 0.0270	5.52×10^{-5}	0.09 ± 0.0055
BP-1	1.57×10^{-8}	0.46 ± 0.0180	8.39×10^{-6}	0.23 ± 0.0012	5.71×10^{-5}	0.10 ± 0.0037
BP-10	6.48×10^{-8}	0.22 ± 0.0068	2.98×10^{-6}	0.30 ± 0.0208	3.27×10^{-5}	0.09 ± 0.0041
BP-15	1.31×10^{-7}	0.22 ± 0.0167	2.39×10^{-6}	0.21 ± 0.0224	3.13×10^{-5}	0.09 ± 0.0029
BP-20	7.41×10^{-8}	0.14 ± 0.0154	2.28×10^{-6}	0.08 ± 0.0115	2.88×10^{-5}	0.08 ± 0.0091

[a]Measured at room temperature.

The linear dependence of $\log\sigma_{ac}$ on $1000/T$ indicates that the ac conductivity is a thermally activated process. The data are fitted to the Arrhenius equation expressed by:

$$\sigma_{ac} = \sigma_o e^{-E_{ac}/k_B T}, \quad (4)$$

where σ_o is a pre-exponential factor, E_{ac} is the activation energy, k_B is the Boltzmann's constant and T is the absolute temperature. The activation energies (E_{ac}) for all samples were calculated from the slopes of the straight lines in Fig. 6 and listed in Table III. It can be noticed that the activation energy values decrease with increasing frequency, which can be attributed to the enhancement of the electronic jumps between the localized states when the applied frequency is increased.[50] Consequently, the conductivity values at room temperature increase with increasing frequency.

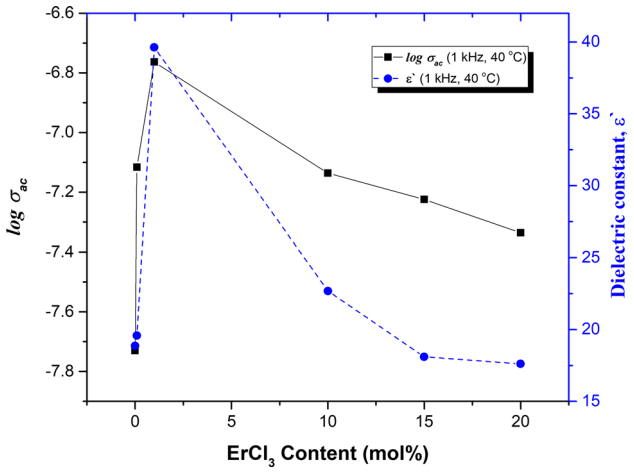

Fig. 7. Variations of the ac conductivity and the dielectric constant at constant frequency (1 kHz) and temperature (40°C) as a function of $ErCl_3$ content in mol.%.

It is reported that when PbO content is higher than 12 mol.%, and the conductivity is measured in the temperature range 487–583 K, lead ions can act as the charge carrier.[51] These charge carriers are expected to have higher activation energies than those calculated in the present investigation (Table III). The lower values of the recorded activation energies are due to the dominance of electronic conduction preceded by the electrons of non-bridging atoms.

It can be noticed from Fig. 6 that the conductivity values increase with the incorporation of the rare earth ion (Er^{3+}), giving an indication that its addition also facilitates the mobility of electrons due to the increase of non-bridging oxygen units and their associated electrons.[52] Therefore, it can be concluded that conduction in the present glasses is due to electronic conduction in addition to ionic conduction by lead and Er^{3+} ions.[51]

The variations of ac conductivity ($\log\sigma_{ac}$) and the dielectric constant (ε') with $ErCl_3$ content at frequency 1 kHz and temperature 40°C are shown in Fig. 7. From this figure, it can be seen that both the ac conductivity and the dielectric constant (ε') increases with the increase in Er^{3+} ions, reaching a maximum at 1 $ErCl_3$ mol.% then decreases with further increase in the $ErCl_3$ content. As previously described, the increase in conductivity can be attributed to the enhancement of the electronic and ionic conductions. However, the increase of Er^{3+} ions above 1 mol.% can hinder the ease migration of the charge carriers leading to a decrease in the conductivity values. It is reported that rare earth elements are considered high field-strength elements.[53] As a result of increasing Er^{3+} ions, a structural contraction occurs due to its high field strength, which explains the observed decrease in the conductivity values above 1 mol.%.[54]

The increase of ε' in Fig. 7 was attributed to the increase of non-bridging oxygen atoms and weakening of the glass network.[52] The weakening of the glass network created pathways, which were suitable for the migration of pb^{2+} and Er^{3+}ions that can participate in the build-up of space charge polarization, thereby resulting to a relatively large value of ε' as observed in Fig. 7. After reaching a maximum at 1 mol.% $ErCl_3$ (Fig. 7), the decrease in ε' at 1 kHz can be attributed to the increase of Er^{3+} ions that result in glass structure contraction.[54]

CONCLUSION

In this study, we have prepared lead borate glasses with composition (mol.%) $70PbO{\cdot}30B_2O_3$ containing different percentages of $ErCl_3$ (0.1, 1, 10, 15 and 20 mol.%). All the studied parameters were found to be dependent on the dopant concentration and the results were explained in the context of the relevant theories.

The glass samples under study are good candidates for magnetic applications. The saturation magnetization increases with increasing the concentration of Er^{3+}, whereas the coercivity remains unchanged. The absorption spectra of the doped glasses revealed the development of absorption bands due to (*f–f*) transitions. The allowed direct energy gap calculated from Tauc plots was found to be correlated with the dopant concentration. The incorporation of $ErCl_3$ into the glass system has found to weaken the glass network up to 1 mol.% $ErCl_3$ due to the increase of the non-bridging oxygen units. This behavior led to a significant enhancement in the electronic and ionic conduction. However, above 1 mol.% $ErCl_3$ contraction in the glass structure may occur due to the high field strength of the rare earth ions. The first weakening of glass network up to 1 mol.% creates pathways suitable for the migration of pb^{2+} and Er^{3+} ions that can participate in the build-up of space charge polarization, thereby resulting in a large increase in ε'. The maximum ε' value reached in the sample with 1 mol.% $ErCl_3$ suggests its application as an energy storage material in electronic devices.

REFERENCES

1. B. Locardi and E. Guadagnino, *Mater. Chem. Phys.* 31, 45 (1992).
2. Y. Tu, S. Zhao, D. He, T. Wu, H. Zhang, R. Lei, L. Huang, and S. Xu, *J. Mater. Chem. C* 6, 7063 (2018).
3. D.D. Ramteke, H.C. Swart, and R.S. Gedam, *J. Rare Earths* 35, 480 (2017).
4. F.A. Abdel-Wahab and H.A. Maksoud, *Am. J. Condens. Matter Phys.* 2017, 41 (2017).
5. M. Farouk, A. Samir, F. Metawe, and M. Elokr, *J. Non Cryst. Solids* 371–372, 14 (2013).
6. E.A. dos Santos, L.C. Courrol, L.R.P. Kassab, L. Gomes, N.U. Wetter, N.D. Vieira, S.J.L. Ribeiro, and Y. Messaddeq, *J. Lumin.* 124, 200 (2007).
7. S. Shen, A. Jha, X. Liu, M. Naftaly, K. Bindra, H.J. Bookey, and A.K. Kar, *J. Am. Ceram. Soc.* 85, 1391 (2002).
8. S. Tanabe, *Photonics Based Wavel. Integr. Manip.* 2, 101 (2005).
9. H. Lin, E.Y.-B. Pun, X. Wang, and X. Liu, *J. Alloys Compd.* 390, 197 (2005).

10. I.-I. Oprea, H. Hesse, and K. Betzler, *Opt. Mater. Amst.* 28, 1136 (2006).
11. P. Babu, H.J. Seo, K.H. Jang, K. Upendra Kumar, and C.K. Jayasankar, *Chem. Phys. Lett.* 445, 162 (2007).
12. S. Xu, Z. Yang, S. Dai, G. Wang, L. Hu, and Z. Jiang, *J. Non Cryst. Solids* 347, 197 (2004).
13. S. Tanabe, *J. Alloys Compd.* 408–412, 675 (2006).
14. K. Pradeesh, C.J. Oton, V.K. Agotiya, M. Raghavendra, and G.V. Prakash, *Opt. Mater. Amst.* 31, 155 (2008).
15. K. Goud, C. Ramesh, and B.A. Rao, *Mater. Sci. Res. India* 14, 140 (2017).
16. D. Rajeshree Patwari and B. Eraiah, in IOP conference series: materials science and engineering 2018.
17. B.V. Padlyak, R. Lisiecki, and W. Ryba-Romanowski, *Opt. Mater. Amst.* 54, 126 (2016).
18. C.R. Kesavulu, H.J. Kim, S.W. Lee, J. Kaewkhao, N. Wantana, S. Kothan, and S. Kaewjaeng, *J. Alloys Compd.* 683, 590 (2016).
19. W.A. Pisarski, J. Pisarska, R. Lisiecki, Ł. Grobelny, G. Dominiak-Dzik, and W. Ryba-Romanowski, *Chem. Phys. Lett.* 472, 217 (2009).
20. A.D. Sontakke, K. Biswas, A. Tarafder, R. Sen, and K. Annapurna, *Opt. Mater. Express* 1, 344 (2011).
21. M. Bhushana Reddy, S. Sailaja, C. Nageswara Raju, and B. Sudhakar Reddy, *J. Opt.* 43, 101 (2014).
22. W.A. Pisarski, T. Goryczka, B. Wodecka-Duś, M. Płońska, and J. Pisarska, *Mater. Sci. Eng. B* 122, 94 (2005).
23. T.A. Hanafy, *J. Appl. Phys.* 112, 034102 (2012).
24. G.S. Said, F.H. Abd-El Kader, M.M. El Naggar, and B.A. Anees, *Carbohydr. Polym.* 65, 253 (2006).
25. M.A.F. Basha and R.M.M. Morsi, *J. Appl. Polym. Sci.* 134, 45220 (2017).
26. R.M.M. Morsi, S. Ibrahim, and M.M. Morsi, *Ceram. Int.* 43, 8306 (2017).
27. M.M. El-Desoky, M.Y. Hassaan, and M.H. El-Kottamy, *J. Mater. Sci. Mater. Electron.* 9, 447 (1998).
28. F.H. Abd El-kader, W.H. Osman, K.H. Mahmoud, and M.A.F. Basha, *Phys. B Condens. Matter* 403, 3473 (2008).
29. J.C. Anderson, K.D. Leaver, R.D. Rawlings, and J.M. Alexander, *Materials Science* (Boston: Springer, 1990), pp. 518–549.
30. R. Dalven, *Introduction to Applied Solid State Physics* (Boston: Springer, 1990), pp. 347–390.
31. H.A. Othman, M.M. Eltabey, S.E. Ibrahim, L.M.S. El-Deen, and M.M. Elkholy, *Phys. B Condens. Matter* 506, 115 (2017).
32. P. Hojati-Talemi, J. Azadmanjiri, and G.P. Simon, *Mater. Lett.* 64, 1684 (2010).
33. T. Iwaki, Y. Kakihara, T. Toda, M. Abdullah, and K. Okuyama, *J. Appl. Phys.* 94, 6807 (2003).
34. H. Gavrila and V. Ionita, *J. Optoelectron. Adv. Mater.* 5, 919 (2003).
35. R.M. Khattab, H.E.H. Sadek, and A.A. Gaber, *Ceram. Int.* 43, 234 (2017).
36. F.H. ElBatal, M.A. Azooz, and A.A. El-Kheshen, *Trans. Indian Ceram. Soc.* 68, 81 (2009).
37. S. Jana, B. Karmakar, and P. Kundu, *Mater Sci Pol.* 25, 1127 (2007).
38. M. Reddy, S. Raju, and N. Veeraiah, *J. Phys. Chem. Solids* 61, 1567 (2000).
39. V. Prajzler, O. Lyutakov, I. Huttel, J. Oswald, and V. Jerabek, *Advances in Lasers and Electro Optics* (Rijeka: In-Tech, 2010).
40. M. Wachtler, A. Speghini, K. Gatterer, H.P. Fritzer, D. Ajò, and M. Bettinelli, *J. Am. Ceram. Soc.* 81, 2045 (1998).
41. G.M. Gurgel, L.X. Lovisa, L.M. Pereira, F.V. Motta, M.S. Li, E. Longo, C.A. Paskocimas, and M.R.D. Bomio, *J. Alloys Compd.* 700, 130 (2017).
42. H. Yuan, J. Zhang, R. Yu, and Q. Su, *J. Rare Earths* 27, 308 (2009).
43. J.H. Nobbs, *Rev. Prog. Color. Relat. Top.* 15, 66 (2008).
44. W.E. Vargas, *J. Opt. A Pure Appl. Opt.* 4, 314 (2002).
45. S. Khan, G. Kaur, and K. Singh, *Ceram. Int.* 43, 722 (2017).
46. J. Tauc, R. Grigorovici, and A. Vancu, *Phys. Status Solidi* 15, 627 (1966).
47. J. Tauc, *Mater. Res. Bull.* 3, 37 (1968).
48. S.B. Mallur, T. Czarnecki, A. Adhikari, and P.K. Babu, *Mater. Res. Bull.* 68, 27 (2015).
49. G.B. Devidas, T. Sankarappa, M. Prashant Kumar, and S. Kumar, *J. Mater. Sci.* 43, 4856 (2008).
50. M.M. El-Nahass, H. Kamal, M.H. Elshorbagy, and K. Abdel-Hady, *Org. Electron. Phys. Mater. Appl.* 14, 2847 (2013).
51. A. Tawansi, I.A. Gohar, D. Holland, and N.A. El-Shishtawi, *J. Phys. D Appl. Phys.* 21, 607 (1988).
52. A.A. Ali and M.H. Shaaban, *Bull. Mater. Sci.* 34, 491 (2011).
53. F. Albarede, *Geochemistry: An Introduction* (Cambridge: Cambridge University Press, 2009).
54. R.M.M. Morsi, S.I. Abd El-Ghany, and M.M. Morsi, *J. Mater. Sci. Mater. Electron.* 26, 1419 (2015).